Microfluid Nanofluid (2016) 20:111
DOI 10.1007/s10404-016-1764-8

RESEARCH PAPER

Approach to analytic solutions for electroosmotic flow in micro-ducts by eigenfunctions of the Helmholtz equation

Chang-Yi Wang[1] · **Chun-Fei Kung**[2,3] · **Chien-Cheng Chang**[2,3]

Received: 1 February 2016 / Accepted: 13 June 2016 / Published online: 13 July 2016

Abstract In the literature, a limited number of analytical solutions for electroosmotic (EO) flow in micro-ducts were obtained. In this study, we present a general formulation using eigenfunctions of the Helmholtz equation to obtain analytic solutions for steady and unsteady EO flow in micro-ducts under Debye–Hückel approximation. The key observation is that the differential operator associated with the equation for the EO flow is strictly positive definite. Examples that add to analytic solutions for EO flow include exact series and closed-form solutions to the steady flow, and the starting flow and the oscillatory flow in three triangular ducts are found. It is easy to deduce some salient features of flow physics, such as the flow rate, transient time and phase lag as well as the velocity profile from the general solution, and they are given quantitative values in the individual examples.

Keywords Electroosmotic flow · Micro-ducts · Starting · Oscillatory · Triangular · Helmholtz equation · Eigenfunctions · Analytic solution

✉ Chun-Fei Kung
d92543012@ntu.edu.tw

✉ Chien-Cheng Chang
mechang@iam.ntu.edu.tw

[1] Departments of Mathematics and Mechanical Engineering, Michigan State University, East Lansing, MI 48824, USA

[2] Center for Advanced Study in Theoretical Sciences and Institute of Applied Mechanics, National Taiwan University, Taipei 106, Taiwan

[3] College of Mechanical Engineering, Guangxi University, Nanning 530004, China

1 Introduction

Electroosmosis has become important in transporting or mixing fluids in MEMS, micro-fluidics and biosensors. The electrolyte can be efficiently driven by applying a steady or time-varying voltage due to the existence of electric double layer (EDL) developed on the wall. The present study is aimed to obtain analytical solutions for EO flow in ducts of some basic shapes, which were not obtained in the literature. Analytic solutions for EO flows are important because not only they reveal properties of basic micro-duct geometries, but also they serve as accuracy standards for approximate solutions, whether numerical or asymptotic. The few analytic solutions for steady EO flows are as follows. The steady EO flow in a parallel plate duct has long been known. Rice and Whitehead (1965) first obtained the closed-form solution to the circular duct and Yang and Li (1998) the series solution to the rectangular duct. The solution to the annular duct was found by Tsao (2000), the semicircular duct by Wang et al. (2008) and the sector duct by Chang and Wang (2009), and the polygonal duct by Wang and Chang (2011). Unsteady electroosmosis in micro-ducts includes starting flow when an axial electric field is suddenly applied, and the oscillatory flow due to an AC field. The previous literature on starting EO flows includes Soderman and Jonsson (1996) and Keh and Tseng (2001) who found exact solutions to the flow in the parallel plate channel and the circular tube. Gillespie et al. (2002) developed a one-dimensional model of coupling Poisson–Nernst–Planck (PNP) and density functional theory (DFT) to calculate ion flux. The starting EO flow in an annulus and a rectangular duct was studied by Chang and Wang (2008) and the sector duct by Chang and Wang (2009). On the other hand, the EO flow due to an AC oscillating applied axial field was considered by Bhattacharyya et al.

(2003) for the circular tube, Campisi et al. (2005) for the rectangular duct, Jian et al. (2010) and Moghadam (2014) for the annular duct. Recently, an analytical approach was presented by Moghadam (2016) to explore the EOF and associated heat transfer in a semi-annular micro-capillary. Another research related to the unsteady flow of fluid through a parallel rotating micro-channel was carried out by Gheshlaghi et al. (2016). Gillespie (2015) examined several different continuum models (i.e., Poisson–Boltzmann) that attempt to include ion size, ion concentrations and surface charges. In addition, with regard to the possible interactions of electroosmotic slip and Navier slip conditions, Goswami and Chakraborty (2011) first derived a general semi-analytical formalism for the implications of electroosmotic flows in the presence of Navier slip, corresponding to micro-channel geometries with complex cross-sectional shapes (elliptic, polygonal, point star-shaped, and annular micro-channel).

All the references mentioned above used the Debye–Hückel approximation for low electric potential. Since the equations are linear, superposition methods such as separation of variables, Laplace transform, Green's functions can be used. Also, the cross-sectional geometries must be described by separable coordinates. We mention that for unsteady EO flow using the nonlinear Poisson–Boltzmann equation, it often requires fully numerical means (Zhang et al. 2006; Kamali and Eslami 2008), patching approximations (Kang et al. 2002) or perturbation method (Chang et al. 2011).

This paper describes an eigenfunction superposition method to solve linear unsteady EO flows in ducts. The only requirement is that for the same cross-sectional geometry there exist a complete set of eigenfunctions for the Helmholtz equation. The process is somewhat similar to the method of Green's functions (Morse and Feshbach 1953; Riley et al. 2006), except that Green's function itself is not needed. Previous reference using such a method include Wakasugi (1961a, b) who studied the buckling of simply supported triangular plates, and Aggarwala and Iqbal (1969) who investigated the heat convection in some triangular ducts. The unsteady oscillatory flow in a right isosceles duct was solved by Tsangaris and Vlachakis (2003). As a matter of fact, flow in a pipe of various geometries is of fundamental interest in viscous flow; see, e.g., Landau and Lifshitz (1987, Sec. 17).

In this study, we consider a parallel EO flow. The longitudinal velocity w' is governed by (see, e.g., Bruus 2008, p. 158)

$$\rho \frac{\partial w'}{\partial t'} = \mu \nabla'^2 w' + \rho_e E(t') \tag{1}$$

Here t' is the time, E is the longitudinal applied electric field, ρ_e is the charge density, ρ and μ are the fluid density and viscosity, respectively. The fluid flow on the wall is required to satisfy the no-slip condition.

On the other hand, we make the Debye–Hückel approximation; namely, the potential for the electric double layer ψ' is related to ρ_e by

$$\rho_e = -\varepsilon \nabla'^2 \psi' = \frac{-2z^2 e^2 n_0}{k_b T} \psi' \tag{2}$$

where z is the valence, e is the electron charge, n_0 is the bulk electrolyte concentration, k_b is the Boltzmann constant and T is the absolute temperature. In particular, we assume a constant permittivity ε throughout the entire micro-duct. The EDL potential ψ' is assumed to have a constant zeta potential ψ_0 on the wall (Stern layer). It is noted that the Debye–Hückel approximation is valid for dilute solution (say, $n_0 < 10^{-3}$ M) of point-like ions when the zeta potential ψ_0 (or the applied voltage across the EDL) is much less than the thermal voltage k_bT/e (see, e.g., Storey et al. 2008). Moreover, due to low solid–liquid interactions, the zeta potential is somewhat smaller for slip flow (Papadopoulos et al. 2012), and thus, one may expect that the Debye–Hückel approximation is valid for most hydrophobic micro-ducts.

Let ψ_0 be the constant potential on the wall, E_0 be the magnitude of the unsteady applied potential and L be a characteristic cross-sectional length. Normalize the variables as follows

$$\psi = \frac{\psi'}{\psi_0}, \quad w = \frac{w'}{-E_0 \varepsilon \psi_0 / \mu}, \quad t = \frac{t'}{\rho L^2 / \mu}, \quad F(t) = \frac{E(t')}{E_0} \tag{3}$$

Equations (1, 2) become

$$w_t = \nabla^2 w + K^2 \psi F(t) \tag{4}$$

$$\nabla^2 \psi = K^2 \psi \tag{5}$$

with the boundary conditions on the wall

$$\psi = 1, w = 0 \tag{6}$$

where

$$K = L/\lambda_D = zeL\sqrt{\frac{2n_0}{\varepsilon k_b T}}, \tag{7}$$

is the important non-dimensional electrokinetic width with λ_D the Debye length of the electric double layer (EDL) for the potential.

It is worth mentioning the typical values of the important parameters in the range of practical applications. For example, $n_0 = 10^{-4}$ M, $T = 288$ K (15 °C), the thermal voltage is $k_b\, T/e = 0.0248$ V ($k_b = 8.62 \times 10^{-5}$ eV K^{-1}), $\varepsilon = 7 \times 10^{-10}$ C^2 J^{-1} m^{-1}, and λ_D is around 3 nm. The potential value of 25 mV (either positive or negative) can be taken as a useful reference that separates low-charged

surfaces from high-charged surfaces. Therefore, the zeta potential $\psi_0 = 2.50$ mV which is within 10 % tolerance of the thermal voltage can be considered a valid case for the Debye–Hückel approximation. On the other hand, it is apparent from the definition that a large value of K denotes a relatively thin electric double layer and vice versa. The capillary electrophoresis applications usually have K at the orders of about 10^3–10^5 with the Debye lengths (λ_D) in the range of about 1–10 nm in a micro-fluidic channel (with characteristic widths: 10–100 μm). A smaller K (with overlapped EDLs) can be produced by fabricating a smaller cross section or decreasing the bulk electrolyte concentration (low n_0). However, for small K, the polarization of water dipoles in the vicinity would also severely alter the permittivity close to the wall. One may also refer to some recent studies for the practical ranges of the dimensional parameters involved (see, e.g., He et al. 2009; Bandopadhyay and Chakraborty 2011, 2013; Kilic and Bazant 2007a, b; Peng and Li 2015; Iglic et al. 2010; Bandopadhyay et al. 2015).

2 General formulation for steady and unsteady electroosmotic flow

An important application of the Helmholtz equation is the vibration of elastic membranes. Existing exact solutions for various membrane shapes have been compiled in the book by Wang and Wang (2014), where the exact eigenvalues and eigenfunctions of isosceles right triangle, equilateral triangle and 30°–60°–90° triangle are given. These solutions will be utilized for our EO flow problems.

We shall first briefly formulate the method for general duct cross sections. Let (λ_j, ϕ_j) be an eigenpair of the two-dimensional Helmholtz equation,

$$\nabla^2\phi_j + \lambda_j\phi_j = 0 \tag{8}$$

with the homogeneous boundary condition on the wall,

$$\phi_j = 0 \tag{9}$$

Namely, λ_j denotes the (positive)jth eigenvalue and ϕ_j the corresponding eigenfunction. The eigenvalues are arranged in the ascending order of their magnitudes: $0 \le \lambda_1 \le \lambda_2 \le \cdots$, (each counted with its algebraic multiplicity). It can be shown that the set of eigenfunctions is complete, and any pair of eigenfunctions corresponding to distinct eigenvalues is mutually orthogonal to each other (Morse and Feshbach 1953).

2.1 Steady flow

Let $\bar{w}$ be the velocity for steady EO flow. Equations (4, 5) reduce to

$$\nabla^2\bar{w} + K^2\psi = \nabla^2(\bar{w} + \psi) = 0 \tag{10}$$

The conditions in (6) gives $\bar{w} + \psi = 1$ on the wall, which must also be satisfied in the entire duct owing to the maximum principle for the Laplace equation (Strauss 2007, p. 154). In other words, we have the identity, $\psi = 1 - \bar{w}$ in the entire duct, and thus,

$$-\nabla^2\bar{w} + K^2\bar{w} = K^2 \tag{11}$$

with $\bar{w} = 0$ on the boundary. Note that Eq. (11), even the homogeneous part, is not the Helmholtz equation. A good advantage of using the eigenfunctions of the Helmholtz equation is that the operator $-\nabla^2 + K^2$ on the LHS of Eq. (11) is fully positive definite. Namely, it is assured that one may invert the operator to obtain the solution for the EO flow w.

First of all, we expand unity in terms of the Helmholtz eigenfunctions

$$1 = \sum_{j=1}^{\infty} a_j\varphi_j \tag{12}$$

Using the orthogonality property, inversion gives the coefficient a_j

$$a_j = \frac{C_j}{D_j}, \quad C_j = \iint \varphi_j \mathrm{d}A, \quad D_j = \iint \varphi_j^2 \mathrm{d}A \tag{13}$$

where the double integrations are over the cross-sectional area. Next, we express also the steady velocity in terms of the eigenfunctions which satisfy the zero boundary conditions

$$\bar{w} = \sum_{j=1}^{\infty} A_j\varphi_j \tag{14}$$

Equations (11, 12, 14) yield the coefficients

$$A_j = \frac{K^2 a_j}{\lambda_j + K^2} \tag{15}$$

where $\lambda_j + K^2(>0)$ is called the signature of the EO flow differential operator $-\nabla^2 + K^2$ [cf. Eq. (11)] associated with the eigenfunction ϕ_j. The steady flow rate is

$$\bar{Q} = \iint \bar{w}\mathrm{d}A = \sum_{j=1}^{\infty} \frac{K^2 C_j^2}{D_j(\lambda_j + K^2)} \tag{16}$$

It is known that for large K (or thin EDL) the velocity in the interior is almost unity and there exists a boundary layer near the wall. If η is the distance pointing inward from the wall, Eq. (11) can be approximated by

$$\bar{w}_{\eta\eta} - K^2\bar{w} = -K^2 \tag{17}$$

with the solution

$$\bar{w} = 1 - e^{-K\eta} \tag{18}$$

Thus, the velocity deficiency per lateral length due to the boundary layer is, asymptotically

$$\int_0^\infty e^{-K\eta} \mathrm{d}\eta = \frac{1}{K} \tag{19}$$

The approximation of the flow rate for large K is thus

$$\bar{Q} = A - \frac{P}{K} \tag{20}$$

where A is the cross-sectional area and P is the perimeter length.

2.2 Starting flow

Consider a suddenly applied constant axial electric field,

$$F(t) = H(t) \tag{21}$$

where $H(t)$ is the unit step function. Let

$$w = \bar{w}(x, y) - \tilde{w}(x, y, t) \tag{22}$$

that is, the transient solution w is written as the difference between the steady-state solution $\bar{w}(x, y)$ and the unsteady part $\tilde{w}(x, y, t)$. The unsteady part, thus defined, can be considered as the "deficit" away from the steady-state solution. The unsteady part of Eq. (4) is therefore simply governed by

$$\tilde{w}_t = \nabla^2 \tilde{w} \tag{23}$$

with the initial condition

$$\tilde{w}|_{t=0} = \bar{w} \tag{24}$$

Apparently the unsteady part in (22) is defined such that it decays as time evolves. By Eqs. (8, 14, 23, 24), the transient solution is

$$\tilde{w} = \sum_{j=1}^{\infty} A_j \varphi_j e^{-\lambda_j t} \tag{25}$$

The analytic solution in terms of the Helmholtz eigenfunctions is then

$$w = \sum_{j=1}^{\infty} \frac{K^2 C_j}{D_j(\lambda_j + K^2)} \varphi_j \left(1 - e^{-\lambda_j t}\right) \tag{26}$$

The instantaneous flow rate is

$$Q = \iint w \mathrm{d}A = \sum_{j=1}^{\infty} \frac{K^2 C_j^2}{D_j(\lambda_j + K^2)} \left(1 - e^{-\lambda_j t}\right) \tag{27}$$

The first eigenvalue λ_1 governs the rate of the EO flow approaching the steady state. For example, to find the time to approach 1 % of the steady state, we set $\lambda_1 t = 5$, or

$$t \approx \frac{5}{\lambda_1} \tag{28}$$

2.3 Oscillatory flow

Next we consider an oscillatory applied electric field $E_0 \cos(\Omega t')$, where Ω is the frequency. Equation (4) then yields, preferably in complex form,

$$w_t = \nabla^2 w + K^2 \psi e^{ist} \tag{29}$$

where $i = \sqrt{-1}$, $s = \Omega L^2/\nu$ is the normalized frequency. Let

$$w = \sum_{j=1}^{\infty} B_j \varphi_j e^{ist} \tag{30}$$

Using $\psi = 1 - \bar{w}$ and Eqs. (14, 29, 30), after some algebra, we obtain the coefficients

$$B_j = \frac{K^2 a_j \lambda_j}{(\lambda_j + K^2)(\lambda_j + is)} \tag{31}$$

Thus, the induced oscillatory velocity is

$$w = \mathrm{Re}\left[\frac{K^2 C_j \lambda_j}{D_j(\lambda_j + K^2)(\lambda_j + is)} \varphi_j e^{ist}\right] \tag{32}$$

The flow rate is

$$\begin{aligned} Q &= \iint w dA = \mathrm{Re} \sum \frac{K^2 C_j^2 \lambda_j}{D_j(\lambda_j + K^2)(\lambda_j + is)} e^{ist} \\ &= G_1 \cos(st) + G_2 \sin(st) \end{aligned} \tag{33}$$

where

$$\begin{aligned} G_1 &= \sum \frac{K^2 C_j^2 \lambda_j^2}{D_j(\lambda_j + K^2)(\lambda_j^2 + s^2)} \\ G_2 &= \sum \frac{K^2 C_j^2 \lambda_j s}{D_j(\lambda_j + K^2)(\lambda_j^2 + s^2)} \end{aligned} \tag{34}$$

The amplitude of the oscillatory flow rate is

$$M = \sqrt{G_1^2 + G_2^2} \tag{35}$$

The phase lag is

$$\beta = \tan^{-1}(G_2/G_1) \tag{36}$$

The results for the steady EO flow in (16), transient flow in (27) and oscillatory flow in (33)–(36) are the general

formulas, and can be explicitly evaluated as long as the eigenpairs λ_j, ϕ_j of the Helmholtz equation for a given shape of duct are known.

2.4 Discussion of the solution of the general formulation

It is conceivable that the key roles of the present method are played by the eigenpairs λ_j, ϕ_j of the Helmholtz equation. Associated with each eigenpair, the differential operator $-\nabla^2 + K^2$ [cf. Eq. (11)] of the EO flow has the signatures $\lambda_j + K^2 (> 0)$. And thus $1/(\lambda_j + K^2)$ is the system response to the component of the unit input in ϕ_j, i.e.,. $a_j = C_j/D_j$, whence yielding the result in (15) for the steady flow [note that the input of Eq. (11) is K^2]. In the cases of transient flow, the system simply responds by an additional factor $1 - e^{-\lambda_j t}$ in each eigencomponent [cf. Eq. (26)]; hence, the first eigenvalue λ_1 of the Helmholtz equation governs the rate of EO flow approaching the steady state. On the other hand, the oscillatory flow responds with a different factor $\frac{\lambda_j}{\lambda_j + is}$ [cf. Eq. (32)] in each eigencomponent, which contributes to the changes in the magnitude as well in the phase change in response to the external forcing e^{ist}. The resultant phase lag is complicated although each $\frac{\lambda_j}{\lambda_j + is}$ is simply coupling between λ_j and s.

The analytical solutions enable us to ascertain several salient features of the flow rates. It must be noted that λ_j, C_j, D_j and ϕ_j as well are all shape factors; they are determined once the geometry of the duct is specified. Given a duct, the steady EO flow rate $\bar{Q} = \iint \bar{w} dA = \sum_{j=1}^{\infty} \frac{K^2 C_j^2}{D_j(\lambda_j + K^2)}$ [Eq. (16)] may only vary with changing the electrokinetic width K. In the limit of small K, all each summand behaves like $\frac{C_j^2}{D_j \lambda_j} K^2$, and thus, the flow rate is small of order K^2. In the limit of large K, the first few summands are approximately $\frac{C_j^2}{D_j \lambda_j}$, which are simply combinations of the geometric factors, and thus, the flow is expected to approach its maximum at very large K. In the intermediate range of K, we expect that the steady flow rate $\bar{Q}$ increases monotonically with increase in K, for there are more and more terms turning from the behavior of $\frac{C_j^2}{D_j \lambda_j} K^2$ to that of $\frac{C_j^2}{D_j \lambda_j}$. Next we examine the transient flow rate $Q = \iint w dA = \sum_{j=1}^{\infty} \frac{K^2 C_j^2}{D_j(\lambda_j + K^2)} \left(1 - e^{-\lambda_j t}\right)$ [Eq. (27)]. It is noted that everything said about the steady flow rate applies to the transient flow rate except that each summand is multiplied by the shape determined transient factor $1 - e^{-\lambda_j t}$. The larger the first eigenvalue λ_1 is, the faster the flow approaches the steady state. Finally, we examine the oscillatory flow, which has the EO flow rate [Eq. (33)],

$$Q = \iint w dA = \mathrm{Re} \sum \frac{K^2 C_j^2 \lambda_j}{D_j(\lambda_j + K^2)(\lambda_j + is)} e^{ist}$$
$$= G_1 \cos(st) + G_2 \sin(st)$$

The facts about the non-shape factor K said above still apply, yet the additional non-shape parameter s reduces the flow rate through all the summands, especially for the modes with $\lambda_j < s$. Thus, we may conclude that the magnitude of the EO flow rate decreases with increase in the external frequency s. The phase lag $\beta = \tan^{-1}(G_2/G_1)$ with G_1, G_2 given in (34) is complicated by all the shape and non-shape parameters. But as s is a common factor to all summands in G_2 (not in G_1), we expect that the phase lag increases with increase in s.

3 Validation of Helmholtz eigenfunction method

The present method is validated by computing the EO flow rates for the circular duct. For this cross section, the solutions were found previously by the method of separation of variables.

3.1 Steady flow

The steady EO flow was found by Rice and Whitehead (1965). The velocity and the flow rate are

$$\bar{w} = 1 - \frac{I_0(Kr)}{I_0(K)} \tag{37}$$

$$\bar{Q} = 2\pi \left[\frac{1}{2} - \frac{I_1(K)}{K I_0(K)} \right] \tag{38}$$

Here the I's denote the modified Bessel functions.

For the circle, our Helmholtz equation gives

$$\lambda_j = k_j^2 \tag{39}$$

where k_j is the jth root of

$$J_0(k_j) = 0 \tag{40}$$

i.e., $\{k_j\} = 2.40483, 5.52008, 8.65373, 11.7915$. The third and higher eigenvalues are well represented by (Abramowitz and Stegun 1970)

$$k_j = \alpha_j + \frac{1}{8\alpha_j} - \frac{124}{3(8\alpha_j)^3} + \cdots, \quad \alpha_j = (j - 1/4)\pi \tag{41}$$

The eigenfunctions are

$$\varphi_j = J_0(k_j r) \tag{42}$$

Equation (13) gives

$$C_j = \frac{2\pi J_1(k_j)}{k_j}, \quad D_j = \pi J_1^2(k_j) \tag{43}$$

From Eq. (16), the steady flow rate is

$$\bar{Q} = 4\pi K^2 \sum_1^\infty \frac{1}{k_j^2(K^2 + k_j^2)} \tag{44}$$

Now the question is: Does Eq. (44) give the same results as Eq. (38)?

Let us first consider some limiting cases. When $K \to 0$, a series expansion for Eq. (38) gives the leading term

$$\bar{Q} = \frac{\pi K^2}{8} \tag{45}$$

On the other hand, Eq. (44) yields

$$\bar{Q} = 4\pi K^2 \sum_1^\infty \frac{1}{k_j^4} \tag{46}$$

But Sneddon (1960), on the zeros of Bessel functions, showed

$$\sum_1^\infty \frac{1}{k_j^4} = \frac{1}{32} \tag{47}$$

Thus, the results given by Eqs. (38) and (44) are identical when $K \to 0$.When $K \to \infty$, Eq. (38) gives

$$\bar{Q} = \pi \tag{48}$$

which is the same as Eq. (44) for large K when we use another Sneddon (1960) identity

$$\sum_1^\infty \frac{1}{k_j^2} = \frac{1}{4} \tag{49}$$

For general values of K, we show numerically the two solutions are equivalent in Table 1.

3.2 Starting flow

The starting flow was solved by Keh and Tseng (2001) using the method of separation of variables. In brief, Eqs. (22–24) are used to obtain

$$\tilde{w} = \sum_1^\infty A_j J_0(k_j r) e^{-k_j^2 t} \tag{50}$$

$$\tilde{w}|_{t=0} = 1 - \frac{I_0(Kr)}{I_0(K)} \tag{51}$$

Inversion gives

$$A_j = \frac{2K^2}{J_1(k_j)(K^2 + k_j^2)} \tag{52}$$

The transient flow rate is integrated

$$\tilde{Q} = 4\pi K^2 \sum_1^\infty \frac{1}{k_j^2(K^2 + k_j^2)} e^{-k_j^2 t} \tag{53}$$

This is exactly the transient part of our Eq. (27), i.e.,

$$Q = 4\pi K^2 \sum_1^\infty \frac{1}{k_j^2(K^2 + k_j^2)} \left(1 - e^{-k_j^2 t}\right) \tag{54}$$

Thus, the two methods are completely equivalent.

3.3 Oscillatory flow

The oscillatory EO flow was previously studied by Bhattacharyya et al. (2003), but we shall derive a simpler form. Let

$$w = u(r) e^{ist} \tag{55}$$

Equation (29) yields

$$u''(r) + u'/r - isu = -K^2 \psi \tag{56}$$

where

$$\psi = 1 - \bar{w} = \frac{I_0(Kr)}{I_0(K)} \tag{57}$$

Since $u(1) = 0$, the solution to Eq. (56) is

$$u = \frac{K^2}{(K^2 - is)} \left[\frac{I_0(\sqrt{is}r)}{I_0(\sqrt{is})} - \frac{I_0(Kr)}{I_0(K)} \right] \tag{58}$$

It follows

$$\begin{aligned} Q &= 2\pi \int_0^1 wrdr = 2\pi \int_0^1 \mathrm{Re}[ue^{ist}]rdr \\ &= G_1 \cos(st) + G_2 \sin(st) \end{aligned} \tag{59}$$

Table 1 Steady EO flow rate for the circular duct

K	1	5	10	50	∞
$\bar{Q}$	0.33684	2.0189	2.5456	3.0172	3.1416
	0.33684*	2.0189*	2.5456*	3.0172*	3.1416*

Values from Eq. (44) are on top and values from Eq. (38) have asterisks

where we have

$$G_1 = 2\pi \int_0^1 \mathrm{Re}[u] r dr$$
$$G_2 = -2\pi \int_0^1 \mathrm{Im}[u] r dr \tag{60}$$

It is quite tedious to handle the integrals in (60) analytically. Instead, we use numerical integration to evaluate the amplitude and phase

$$M = \sqrt{G_1^2 + G_2^2}, \quad \beta = \tan^{-1}(G_2/G_1) \tag{61}$$

On the other hand, Eq. (34) gives

$$G_1 = 4\pi K^2 \sum_1^\infty \frac{k_j^2}{(K^2 + k_j^2)(s^2 + k_j^2)}$$
$$G_2 = 4\pi K^2 \sum_1^\infty \frac{s}{(K^2 + k_j^2)(s^2 + k_j^2)} \tag{62}$$

The amplitude and phase are then evaluated by Eq. (25). Table 2 shows a comparison of Eq. (60) form separation of variables and Eq. (62) from the Helmholtz eigenfunctions. We see that except for small numerical errors in the fifth digit, the values are identical.

In conclusion, the two methods show identical results. For the steady EO flow, the separation of variables method is more convenient than the Helmholtz eigenfunction method. For oscillatory EO flow, the Helmholtz eigenfunction method is more convenient. For starting EO flow, both methods are equivalent.

However, we emphasize that for the three triangular ducts studied in this paper, the separation of variables method fails, and only the Helmholtz eigenvalue method is successful.

4 Examples: three triangular ducts

4.1 The isosceles right triangular duct

Figure 1a shows the cross section of the isosceles right triangular duct which has a short side as the length scale. The eigenvalues and eigenfunctions are

$$\lambda_{mn} = \pi^2(m^2 + n^2)$$
$$\varphi_{mn} = \sin(n\pi x)\sin(m\pi y) - \sin(m\pi x)\sin(n\pi y) \tag{63}$$

where m, n are non-equal, positive integers. Since λ_{mn} are distinct, $m > n > 0$. Notice the solution Eq. (63) is equivalent, but somewhat simpler, than the form given by Tsangaris and Vlachakis (2003). Equation (13) gives

$$C_{mn} = \frac{4}{(m^2 - n^2)\pi^2} \begin{cases} m/n, & m\ even, n\ odd \\ n/m, & m\ odd, n\ even \\ 0, & m + n = even \end{cases} \tag{64}$$

$$D_{mn} = \frac{1}{4} \tag{65}$$

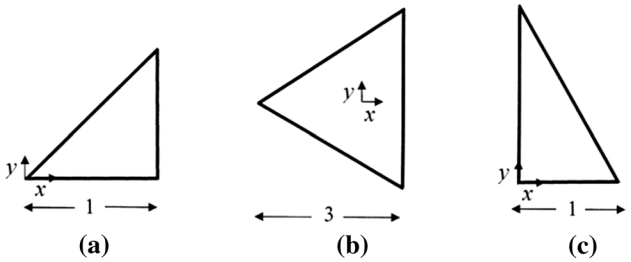

Fig. 1 Three triangular cross sections: **a** Isosceles right triangular duct, **b** equilateral triangular duct, **c** 30°–60°–90° duct. Locations of Cartesian axes are shown

Table 2 Amplitude M and phase β

	s	0	5	10	50	100
$K = 1$	M	0.3368 0.3368*	0.2562 0.2562*	0.1720 0.1720*	0.04492 0.04492*	0.02395 0.02395*
	β	0 0*	0.6784 0.6784*	0.9823 0.9823*	1.3370 1.3370*	1.4078 1.4078*
$K = 10$	M	2.3457 2.5456*	1.9762 1.9762*	1.3960 1.3960*	0.5054 0.5054*	0.3105 0.3105*
	β	0 0*	0.5752 0.5752*	0.7990 0.7990*	1.0464 1.0464*	1.1366 1.1366*
$K = 100$	M	3.0790 3.0790*	2.4314 2.4314*	1.7846 1.7847*	0.8002 0.8002*	0.5623 0.5623*
	β	0 0*	0.4959 0.4959*	0.6616 0.6615*	0.7770 0.7770*	0.8131 0.8130*

Values from Eq. (62) are on top, and values from Eq. (60) have asterisks

The steady-state velocity distribution solution is given by Eq. (14). Figure 2 shows that the velocity profile is rounded for low K (thick EDL) but turns into a plateau for large K (thin EDL). The flow rate is shown in Fig. 3. Since the steady EO flow for this triangular duct is derived for the first time, numerical values are given in Table 3 as benchmarks. Here, we use 16 terms to achieve excellent convergence in the series expansion (16). We see the boundary layer approximation Eq. (20), which is valid for large K, compares very well with our exact solution for high K. For less than 1 % error, K should be larger than 40.

The solution to starting flow is given by Eqs. (26, 27). The velocity distribution for low K is quasi-steady, rounded as shown in Fig. 2a. Figure 4 shows typical instantaneous velocity distributions for a high K, where we see, at small times, the EDL near the boundary first induces the flow forward, and the interior velocity catches up only later. Figure 5 shows the unsteady flow rate for starting EO flow. From Eq. (63), the first (lowest) eigenvalue is $5\pi^2$, and Eq. (28) shows the time to reach steady state is about 0.1, which is indeed the case.

The velocity profiles for low frequency are almost in phase with the external applied potential. Figure 6 shows the velocity profiles for large frequency, while Fig. 7 shows the magnitudes and phase lags for various frequencies. Not only there is a phase lag, but also the maximum velocity is in the boundary layer near the walls (Fig. 6 at $st = 0$ and $3\pi/4$), which is equivalent to the "annular effect" for viscous flow in circular ducts (Schlichting 1979).

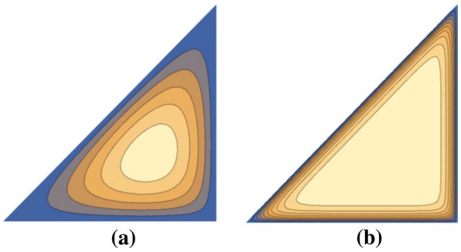

Fig. 2 Steady velocity distribution for the isosceles triangular duct: **a** $K = 1$ velocity from outside: 0, 0.005, 0.01, 0.015, 0.02, 0.025 max 0.026, **b** $K = 30$ velocity from outside: 0, 0.1, 0.2, 0.3, 0.4, 0.5, 0.6, 0.7, 0.8, 0.9 max 0.999

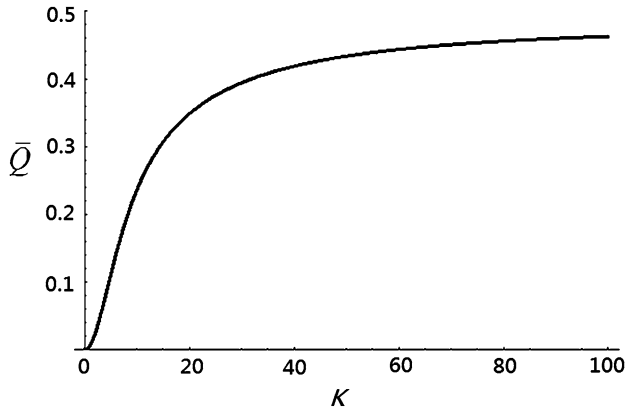

Fig. 3 Steady flow rate $\bar{Q}$ versus K for the isosceles triangular duct

Table 3 Steady-state EO flow rate for the isosceles right triangular duct

K	$\bar{Q}$ exact Eq. (16)	$\bar{Q}$ approx Eq. (20)
1	0.006401	
10	0.2366	0.1586
20	0.3486	0.3293
40	0.4187	0.4146
60	0.4435	0.4431
80	0.4557	0.4573
100	0.4628	0.4659
∞	0.5000	0.5000

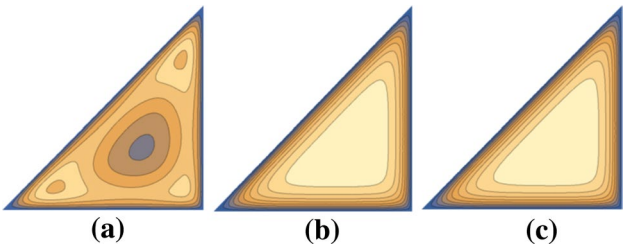

Fig. 4 Velocity distribution for starting flow in an isosceles triangular duct, $K = 20$. **a** $t = 0.01$, velocity from outside = 0, 0.1, 0.2, 0.3, 0.4, 0.5, 0.6, max near sharp corner 0.610, depression near center 0.263, **b** $t = 0.1$, max velocity near center 0.979, **c** $t = 1$, max velocity near center 0.992

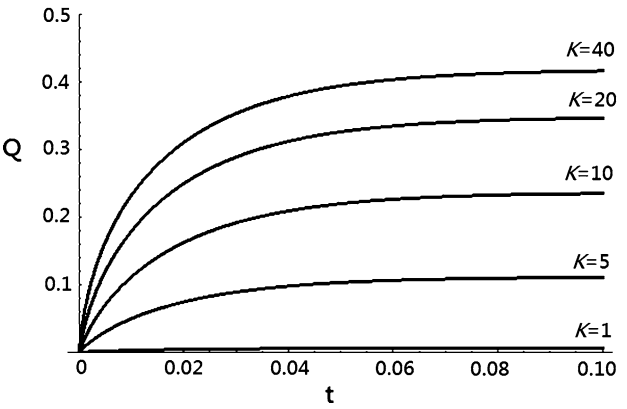

Fig. 5 Unsteady flow rate Q versus time t for the isosceles triangular duct. From top, $K = 40, 20, 10, 5, 1$

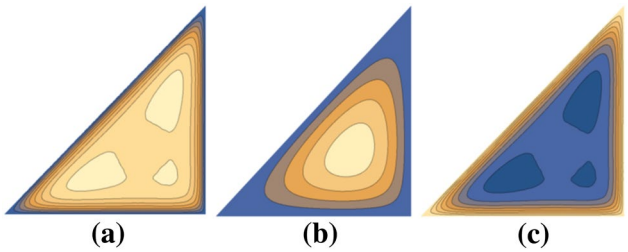

Fig. 6 Instantaneous velocity profiles for the isosceles right triangular duct. $K = 20$, $s = 20$. **a** $st = 0$, instantaneous velocity from outside = 0, 0.1, 0.2, 0.3, 0.4, 0.5, 0.6, 0.7, 0.81, max near corner 0.83, **b** $st = 0.5\pi$, instantaneous velocity from outside = 0, 0.1, 0.2, 0.3, 0.4, max near center 0.457, **c** $st = \pi$, instantaneous velocity from outside = 0, −0.1,−0.2, −0.3, −0.4, −0.5, −0.6, −0.7, −0.81, min near corner—0.83, local max near center—0.791

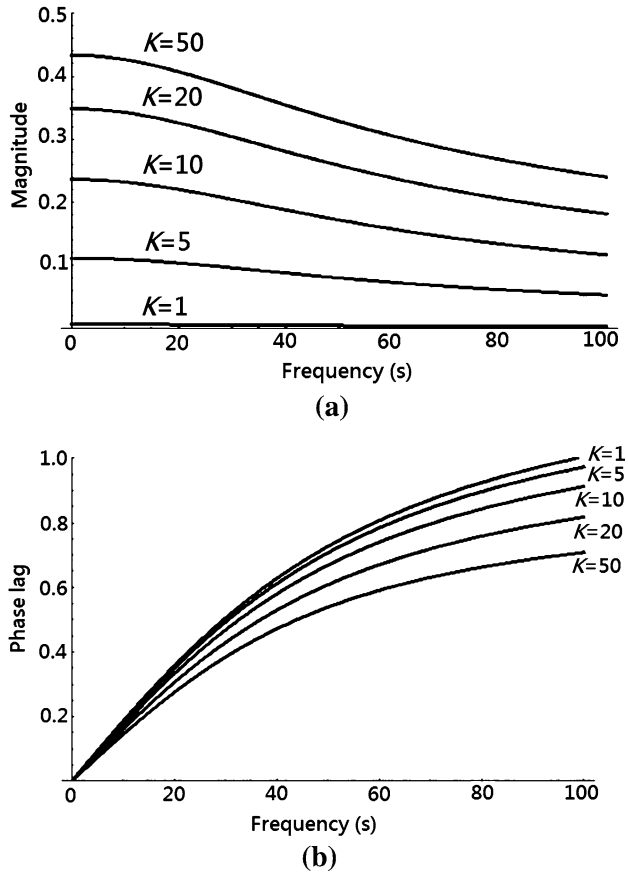

Fig. 7 Oscillatory flow rate for EO flow in an isosceles right triangular duct. **a** Magnitude versus frequency s. From *top* $K = 50$, 20, 10, 5, 1. **b** Phase lag versus frequency. From *top* $K = 1$, 5, 10, 20, 50

4.2 The equilateral triangular duct

Figure 1b shows the cross section of the equilateral triangular duct where the length scale is one third of the triangle height. Let us place the origin of the Cartesian coordinates at the centroid. The boundaries are at

$$x = 1, y = \pm(x+2)/\sqrt{3} \tag{66}$$

Schelkunoff (1943) gave the eigenfunctions for the Helmholtz equation inside the equilateral triangular region, which in our variables is

$$\begin{aligned}\varphi_{mn} = &\cos\left[\frac{(m+2n)\pi y}{3\sqrt{3}}\right]\sin\left[\frac{m\pi(2+x)}{3}\right]\\ &-\cos\left[\frac{(m-n)\pi y}{3\sqrt{3}}\right]\sin\left[\frac{(m+n)\pi(2+x)}{3}\right]\\ &+\cos\left[\frac{(2m+n)\pi y}{3\sqrt{3}}\right]\sin\left[\frac{n\pi(2+x)}{3}\right]\end{aligned} \tag{67}$$

with the eigenvalues

$$\lambda_{mn} = \frac{4\pi^2}{27}\left(m^2+mn+n^2\right) \tag{68}$$

Here m and n are integers which are nonzero, and do not add up to zero. Schelkunoff's solution is symmetric about the x-axis. The solution for fluid flow is more restricted, that it must also have threefold rotational symmetry. A rotation of 120° about the origin is given by the transform

$$\bar{x} = -x/2 - \sqrt{3}y/2, \bar{y} = \sqrt{3}x/2 - y/2 \tag{69}$$

We require

$$\varphi_{mn}(x,y) = \varphi_{mn}(\bar{x},\bar{y}) \tag{70}$$

This yields the restriction

$$\begin{aligned}&m\cos\left(\frac{2m\pi}{3}\right) - (m+n)\cos\left(\frac{2(m+n)\pi}{3}\right)\\ &+ n\cos\left(\frac{2n\pi}{3}\right) = 0\end{aligned} \tag{71}$$

We also found, for $m \neq n$,

$$\iint \varphi_{mn} dA = 0 \tag{72}$$

Thus, the only admissible integers are $m = n = 1, 2, 3,\ldots$, from which we find

$$C_{nn} = \frac{9\sqrt{3}}{n\pi}, \quad D_{nn} = \frac{9\sqrt{3}}{2} \tag{73}$$

Let $\varphi_j = \varphi_{jj}$, the eigenfunctions and eigenvalues are simplified to

$$\phi_j = 2\cos\left(\frac{j\pi y}{\sqrt{3}}\right)\sin\left(\frac{j\pi(2+x)}{3}\right) - \sin\left(\frac{2j\pi(2+x)}{3}\right) \tag{74}$$

$$\lambda_j = \frac{4j^2\pi^2}{9} \tag{75}$$

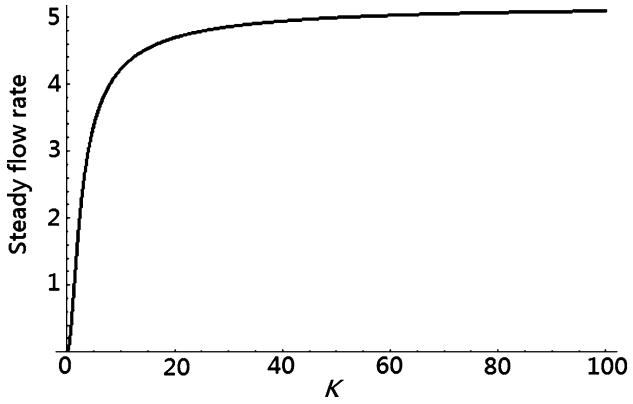

Fig. 8 Steady flow rate versus K for the equilateral triangular duct

The steady-state velocity is simplified to

$$\bar{w} = \sum_{j=1}^{\infty} \frac{2K^2}{j\pi(\lambda_j + K^2)} \varphi_j \tag{76}$$

Typical profiles are similar to those shown in Fig. 2. The steady flow rate, from Eq. (16), is

$$\bar{Q} = \frac{162\sqrt{3}K^2}{\pi^2} \sum_{j=1}^{\infty} \frac{1}{j^2(4\pi^2 j^2 + 9K^2)} \tag{77}$$

We are fortunate that Eq. (77) can be summed into closed form (e.g., Jolly 1961)

$$\bar{Q} = \frac{\sqrt{3}}{K^2}\left[4 + 3K^2 - 6K \coth\left(\frac{3K}{2}\right)\right] \tag{78}$$

Equation (78) is shown in Fig. 8. Table 4 shows a comparison of this exact result with those of Wang and Chang (2011) who used a semi-numerical point match method. Here, again we use 16 terms to achieve excellent convergence in the series expansion (78).

Table 4 Steady-state EO flow rate for the equilateral triangular duct

K	$\bar{Q}$ exact Eq. (78)	$\bar{Q}$ Point match Wang and Chang (2011)	$\bar{Q}$ approx Eq. (20)
1	0.64303	0.643	
2	1.7062	1.706	
5	3.3948	3.395	3.118
10	4.2262	4.226	4.157
20	4.6939	4.694	4.677
50	4.9911	4.991	4.988
∞	5.1962	5.196	5.196

The steady flow rate for $K = \infty$ is the cross-sectional area $3\sqrt{3}$.

The solution to starting flow is given by Eqs. (26, 27). Typical velocity profiles are similar to those of the isosceles right triangular duct and are not presented in this paper. Figure 9 shows the flow rate for starting EO flow. Since the lowest eigenvalue is $\lambda_1 = 4\pi^2/9$, the time to approach steady state is approximately 1.1 which is indeed reflected in the figure. For oscillatory flow, the amplitude and phase lag, as given by Eqs. (35, 36) are shown in Fig. 10.

4.3 The 30°–60°–90° triangular duct

Figure 1c shows the cross section. The length scale used is the short side. The solution to the corresponding Helmholtz equation was found by Seth (1947), which in our formulation the eigenfunctions are

$$\begin{aligned}\varphi_{mn} = &\cos\left[\frac{(3+2m+4n)\pi}{6}(3+2x)\right]\cos\left[\frac{(1+2m)\pi}{2}\left(1+\frac{2y}{\sqrt{3}}\right)\right] \\ &-\cos\left[\frac{(3+2n+4m)\pi}{6}(3+2x)\right]\cos\left[\frac{(1+2n)\pi}{2}\left(1+\frac{2y}{\sqrt{3}}\right)\right] \\ &+\sin\left[\frac{(m-n)\pi}{3}(3+2x)\right]\sin\left[(1+m+n)\pi\left(1+\frac{2y}{\sqrt{3}}\right)\right]\end{aligned} \tag{79}$$

The eigenvalues are

$$\lambda_{mn} = \frac{4\pi^2}{9}[4(m^2+mn+n^2)+6(m+n)+3] \tag{80}$$

Here $m > 0$, $m \neq n$, and $m \geq |n|$. In terms of increasing eigenvalues (increasing j), the (m, n) pairs are (1, −1), (1, 0), (2, −2), (2, −1), (2, 0), (3, −2), (3, −3), (3, −1), (2, 1), (3, 0), (4, −3), (4, −2), (4, −4), (4, −1), (3, 1), (4, 0), etc.

We find

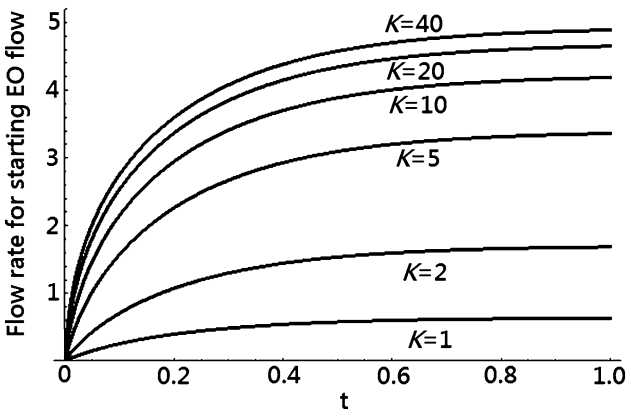

Fig. 9 Flow rate for starting EO flow in an equilateral triangular duct. From *top* $K = 40, 20, 10, 5, 2, 1$

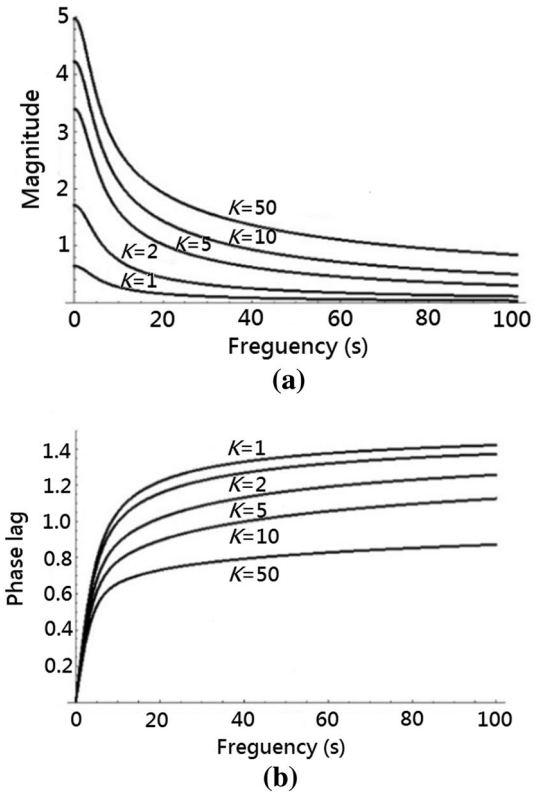

Fig. 10 Oscillatory flow rate for EO flow in an equilateral triangular duct. **a** Magnitude versus frequency s. From *top* $K = 50, 10, 5, 2, 1$. **b** Phase lag versus frequency. From *top* $K = 1, 2, 5, 10, 50$

Table 5 Steady-state EO flow rate for the 30°–60°–90° triangular duct

K	$\bar{Q}$ exact Eq. (16)	$\bar{Q}$ approx. Equation (20)
1	0.01729	
5	0.2586	
10	0.4798	0.3928
20	0.6511	0.6294
50	0.7742	0.7714
100	0.8174	0.8187
∞	0.8660	0.8660

The steady-state solution flow rate, given by Eq. (16), is shown in Fig. 11. Table 5 gives the numerical values. Here we also use 16 terms to achieve excellent convergence in the series expansion (16). The $K = \infty$ limit is the area $\sqrt{3}/2$.

Figure 12 shows the starting EO flow rate versus time. Since the lowest eigenvalue is $\lambda_1 = 28\pi^2/9$, the time to approach steady state is approximately $5/\lambda_1 \approx 0.16$, which is reflected in Fig. 12. For oscillatory EO flow, the magnitude and the phase lag are shown in Fig. 13.

5 Concluding remarks

In this study, we have presented a general procedure of using eigenpairs of the Helmholtz equation for solving

$$C_{mn} = \frac{3\sqrt{3}}{\pi^2}\left\{\begin{array}{l} \frac{1+(-1)^n\cos[(2m+n)\pi/3]}{(1+2n)(3+4m+2n)} - \frac{1-(-1)^{m+n}\cos[(m-n)\pi/3]}{4(m-n)(1+m+n)} \\ -\frac{1+(-1)^m\cos[(m+2n)\pi/3]}{(1+2m)(3+2m+4n)} \\ +\frac{(3+2m+4n)\langle 1-\cos[2(m+2n)\pi/3]\rangle}{8(1+2m)(m-n)(3+4m+2n)} \\ +\frac{(3+4m+2n)\langle 1+\cos[(3+4m+2n)\pi/3]\rangle}{8(1+2n)(m-n)(3+2m+4n)} \\ -\frac{1-\cos[2(n-m)\pi/3]}{8(1+m+n)(3+2m+4n)} + \frac{1+\sin[(9-4m+4n)\pi/6]}{8(1+m+n)(3+4m+2n)} \end{array}\right\} \tag{81}$$

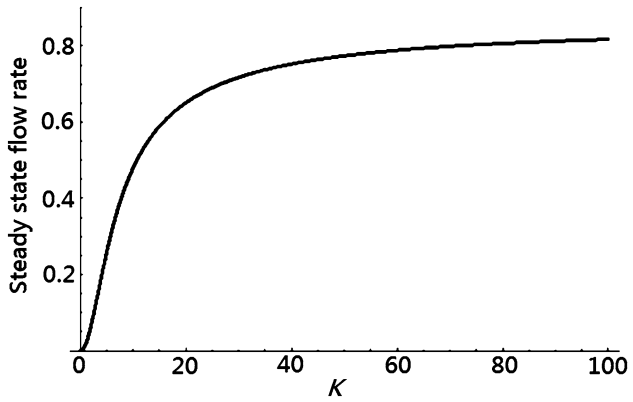

Fig. 11 Steady-state flow rate versus K for the 30°–60°–90° duct

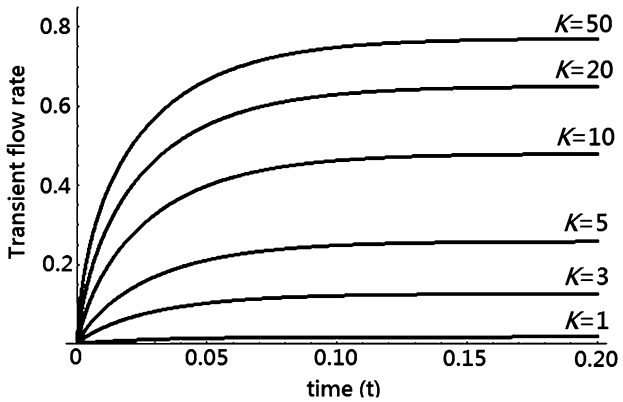

Fig. 12 Transient flow rate versus time t for the 30°–60°–90° duct. From *top* $K = 50, 20, 10, 5, 3, 1$

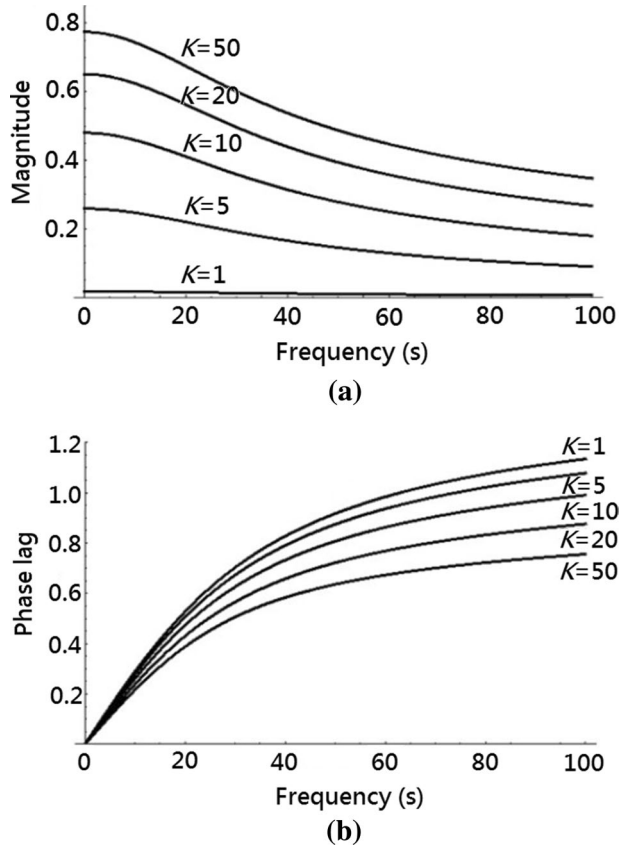

Fig. 13 Oscillatory flow rate for EO flow in a 30°–60°–90° triangular duct. **a** Magnitude versus frequency s. From *top* $K = 50, 20, 10, 5, 1$. **b** Phase lag versus frequency. From *top* $K = 1, 5, 10, 20, 50$

EO flow in micro-ducts. The solutions are exact series solutions (some of which are in closed form) under the Debye–Hückel approximation. The method has only the requirement that the eigenvalues and eigenfunctions of the Helmholtz equation can be found for the duct.

The ducts to which the present method of solution is applicable include a variety of shapes whose boundaries are given in separable coordinates. However, the EO flows for these shapes (rectangle, sector, annulus, etc.) are more easily obtained by the method of separation of variables. Thus, the method of using the Helmholtz eigenfunctions is most suitable for cross sections which are not describable in separable coordinates. The three examples of triangular shapes discussed in this paper have these properties. Nonetheless, the method of using Helmholtz eigenfunctions is first validated for the EO flow in a circular duct.

The solution in the general formulation enables us to identify general behaviors of the flow rates before proceeding with detailed examples. It is the definite signature of the differential operator of EO flow that explains the success of the Helmholtz eigenfunction method in obtaining convergent series solutions. The EO flow is characterized by the eigenfunctions of the Helmholtz equations, the electrokinetic width K as well as the external forcing frequency s (only for the oscillatory flow). For obvious reasons, the eigenfunctions are shape factors, while K and s are non-shape physical factors. Given the geometry of the duct, the trend of the steady flow rate is determined by the relative importance of λ_j and K^2. For the transient flow, the rate with which the EO flow approaches the steady state is governed by the first eigenvalue of the Helmholtz equation. For the oscillatory flow, the magnitude of the EO flow rate decreases with increasing the external frequency s, while the phase lag β is complicated by all the geometric and physical factors. In general, β increases with increasing s. At large external frequency s, not only there is a phase lag, but also the maximum velocity in the boundary layer is closer to the walls.

The three examples of triangular shapes, besides their technical contents, not only concretely add to new analytical solutions for EO flow in ducts, but also testify all the salient features revealed from the analytical solutions in the general formulation. The general formulation applies to cases whether the eigenfunctions can be obtained analytically (say, by numeric methods) or not. Nevertheless, the geometries of triangular ducts considered here are not readily amenable to the current fabrication techniques. The present work stands from a completely theoretical point of view that the choice of test cases (for other numerical or experimental methods) can be justified.

As a final remark, in a wider range of applications with the ratio $\lambda = ze\psi_0/k_bT$ being not small but close to 1, the DHA is no longer valid and one may resort to the analysis of the Poisson–Boltzmann equation. Nevertheless, in the line of our previous approach (Chang et al. 2011), the present DHA solution provides the base for extension of analysis to the Poisson–Boltzmann equation, or the more general Poisson–Nernst–Planck equations. In other realistic applications, one may need more accurate model to account for the physics and chemistry.

Acknowledgments The work was supported in part by the Ministry of Science and Technology (Taiwan). Part of the work was completed while C.C. Chang was visiting Guangxi University.

References

Abramowitz M, Stegun IA (1970) Handbook of mathematical functions. Dover, New York

Aggarwala BD, Iqbal M (1969) On limiting Nusselt numbers from membrane analogy for combined free and forced convection through vertical ducts. Int J Heat Mass Trans 12:737–748

Bandopadhyay A, Chakraborty S (2011) Steric-effect induced alterations in streaming potential and energy transfer efficiency of non-newtonian fluids in narrow confinements. Langmuir 27:12243–12252

Bandopadhyay A, Chakraborty S (2013) Ionic size dependent electroosmosis in ion-selective microchannels and nanochannels. Electrophoresis 34:2193–2198

Bandopadhyay A, Shaik VA, Chakraborty S (2015) Effects of finite ionic size and solvent polarization on the dynamics of electrolytes probed through harmonic disturbances. Phys Rev E 91:042307

Bhattacharyya A, Masliyah JH, Yang J (2003) Oscillating laminar electrokinetic flow in infinitely extended circular microchannels. J Colloid Interface Sci 261:12–20

Bruus H (2008) Theoretical microfluidics. Oxford University Press, New York

Campisi M, Accoto D, Dario P (2005) AC electroosmosis in rectangular microchannels. J Chem Phys 123:204724

Chang CC, Wang CY (2008) Starting electroosmotic flow in an annulus and in a rectangular channel. Electrophoresis 29:2970–2979

Chang CC, Wang CY (2009) Electro-osmotic flow in a sector microchannel. Phys Fluids 21:042002

Chang CC, Kuo CY, Wang CY (2011) Unsteady electroosmosis in a microchannel with Poisson–Boltzmann charge distribution. Electrophoresis 32:3341–3347

Gheshlaghi B, Nazaripoor H, Kumar A, Sadrzadeh M (2016) Analytical solution for transient electroosmotic flow in a rotating microchannel. RSC Adv 6:17632

Gillespie D (2015) A review of steric interactions of ions: why some theories succeed and others fail to account for ion size. Microfluid Nanofluid 18:717–738

Gillespie D, Nonner W, Eisenberg RS (2002) Coupling Poisson–Nernst–Planck and density functional theory to calculate ion flux. J Phys Condens Matter 14:12129–12145

Goswami P, Chakraborty S (2011) Semi-analytical solutions for electroosmotic flows with interfacial slip in microchannels of complex cross-sectional shapes. Microfluid Nanofluid 11:255

He Y, Gillespie D, Boda D, Vlassiouk I, Eisenberg RS, Siwy ZS (2009) Tuning transport properties of nanofluidic devices with local charge inversion. J Am Chem Soc 131:5194–5202

Iglič A, Gongadze E, Bohinc K (2010) Excluded volume effect and orientational ordering near charged surface in solution of ions and Langevin dipoles. Bioelectrochemistry 79:223–227

Jian Y, Yang L, Liu Q (2010) Time periodic electro-osmotic flow through a microannulus. Phys Fluids 22:042001

Jolly LBW (1961) Summation of series, 2nd edn. Dover, New York

Kamali R, Eslami M (2008) A numerical investigation of transient electro-osmotic flow in rectangular microchannels: a comparison of different models. J Mech Eng Sci 224:1655–1663

Kang Y, Yang C, Huang X (2002) Dynamic aspects of electroosmotic flow in a cylindrical capillary. Int J Eng Sci 40:2203–2221

Keh HJ, Tseng HC (2001) Transient electrokinetic flow in fine capillaries. J Colloid Interface Sci 242:450–459

Kilic MS, Bazant MZ (2007a) Steric effects in the dynamics of electrolytes at large applied voltages. I. Double-layer charging. Phys Rev E 75:021502

Kilic MS, Bazant MZ (2007b) Steric effects in the dynamics of electrolytes at large applied voltages. II. Modified Poisson–Nernst–Planck equations. Phys Rev E 75:021503

Landau LD, Lifshitz EM (1987) Fluid mechanics, 2nd edn. Pergamon Press, New York

Moghadam AJ (2014) Effect of periodic excitation on alternating current electroosmotic flow in a microannular channel. Eur J Mech/B Fluids 48:1–12

Moghadam AJ (2016) Exact solution of electroviscous flow and heat transfer in a semi-annular microcapillary. J Heat Transf 138:011702

Morse PM, Feshbach H (1953) Methods of theoretical physics. McGraw-Hill, New York

Papadopoulos P, Deng X, Vollmer D, Butt HJ (2012) Electrokinetics on superhydrophobic surfaces. J Phys Condens Matter 24:464110

Peng R, Li D (2015) Effects of ionic concentration gradient on electroosmotic flow mixing in a microchannel. J Colloid Interface Sci 440:126–132

Rice CL, Whitehead R (1965) Electrokinetic flow in a narrow cylindrical capillary. J Phys Chem 69:4017–4024

Riley KF, Hobson MP, Bence SJ (2006) Mathematical methods for physics and engineering, 3rd edn. Cambridge University Press, Cambridge

Schelkunoff SA (1943) Electromagnetic waves. Van Nostrand, New York

Schlichting H (1979) Boundary layer theory, 7th edn. McGraw-Hill, New York

Seth BR (1947) Transverse vibrations of rectilinear plates. Proc Indian Acad Sci A25:25–29

Sneddon IN (1960) On some infinite series involving the zeros of Bessel functions of the first kind. Proc Glasgow Math Assoc 4:144–156

Soderman O, Jonsson B (1996) Electro-osmosis: velocity profiles in different geometries with both temporal and spatial resolution. J Chem Phys 105:10300–10311

Storey BD, Edwards LR, Kilic MS, Bazant MZ (2008) Steric effects on ac electro-osmosis in dilute electrolytes. Phys Rev E 77:036317

Strauss WA (2007) Partial differential equations–an introduction, 2nd edn. Wiley, New York

Tsangaris S, Vlachakis NW (2003) Exact solution of the Navier-Stokes equations for the oscillating flow in a duct of cross section of right angled isosceles triangle. Z Angew Math Phys 54:1094–1100

Tsao HK (2000) Electro-osmotic flow through an annulus. J Colloid Interface Sci 225:247–250

Wakasugi S (1961a) Buckling of a simply supported triangular plate having inner angles of 30, 60, 90 degrees. Bull Jpn Soc Mech Eng 4:16–20

Wakasugi S (1961b) Buckling of a simply supported equilateral triangular plate. Bull Jpn Soc Mech Eng 4:20–25

Wang CY, Chang CC (2011) Electroosmotic flow in polygonal ducts. Electrophoresis 32:1268–1272

Wang CY, Wang CM (2014) Structural vibration: exact solutions for strings, membranes, beams and plates. CRC Press, Boca Raton

Wang CY, Liu YH, Chang CC (2008) Analytical solution of electroosmotic flow in a semicircular microchannel. Phys Fluids 20:063105

Yang C, Li D (1998) Analysis of electrokinetic effects on the liquid flow in rectangular microchannels. Colloids Surf A143:339–353

Zhang Y, Wong TN, Yang C (2006) Dynamic aspects of electroosmotic flow. Microfluid Nanofluid 2:205–214